

# A neutron scattering study of two-magnon states in the quantum magnet copper nitrate

D. A. Tennant<sup>1,2,3,4</sup>, C. Broholm<sup>5,6</sup>, D. H. Reich<sup>7</sup>, S. E. Nagler<sup>3</sup>, G. E. Granroth<sup>3</sup>, T. Barnes<sup>7,8</sup>, K. Damle<sup>9</sup>, G. Xu<sup>5</sup>, Y. Chen<sup>5</sup>, and B. C. Sales<sup>3</sup>.

<sup>1</sup>*ISIS Facility, Rutherford Appleton Laboratory, Didcot OX11 0QX, Oxon., United Kingdom*

<sup>2</sup>*Oxford Physics, Clarendon Laboratory, Parks Road, Oxford OX1 3PU, United Kingdom*

<sup>3</sup>*Solid State Division, Oak Ridge National Laboratory, Oak Ridge, TN 37831-6393*

<sup>4</sup>*Dept. of Physics and Chemistry, Risø National Laboratory, Roskilde, DK-4000, Denmark*

<sup>5</sup>*Department of Physics and Astronomy, The Johns Hopkins University, Baltimore, MD 21218*

<sup>6</sup>*NIST Center for Neutron Research, National Institute of Standards and Technology, Gaithersburg, MD 20899*

<sup>7</sup>*Department of Physics and Astronomy, University of Tennessee, Knoxville, TN 37996-1501 and*

<sup>8</sup>*Physics Division, Oak Ridge National Laboratory, Oak Ridge, TN 37831-6373*

<sup>9</sup>*Physics Department, Harvard University, Cambridge, MA 02138*

(Dated: September 18, 2018)

We report measurements of the two-magnon states in a dimerized antiferromagnetic chain material, copper nitrate ( $\text{Cu}(\text{NO}_3)_2 \cdot 2.5\text{D}_2\text{O}$ ). Using inelastic neutron scattering we have measured the one and two magnon excitation spectra in a large single crystal. The data are in excellent agreement with a perturbative expansion of the alternating Heisenberg Hamiltonian from the strongly dimerized limit. The expansion predicts a two-magnon bound state for  $q \sim (2n+1)\pi d$  which is consistent with the neutron scattering data.

PACS numbers: 75.10.Jm, 75.40.Gb, 78.70.Nx

## INTRODUCTION

The basic physics of the elementary one-magnon excitations of lower-dimensional quantum antiferromagnets can now be regarded as well established, both theoretically and experimentally through studies of materials that are reasonably accurate realizations of the spin Hamiltonians. In contrast, higher excitations such as multimagnon continua and bound states have attracted relatively little attention. This topic may prove to be a fascinating area for the application of few- and many-body techniques, and will involve interesting and non-trivial results in band structure, band mixing, bound state formation, phase transitions through the formation of condensates of magnetic excitations [1, 2, 3, 4, 5, 6, 7], and other collective phenomena.

Although some aspects of the physics of low-lying multimagnon states can be inferred from model Hamiltonians using standard theoretical techniques, few experimental studies of these higher excitations have been reported to date. Experimental difficulties that have precluded such work include relatively weak couplings of probes to these higher excitations, dominant contributions from the lowest one-magnon excitations, and resolution requirements in energy and wavenumber that are beyond the capabilities of most techniques.

High-resolution inelastic neutron scattering should prove to be an ideal technique for observing some of these higher magnetic excitations. One can control both energy and momentum transfer, so that the existence and spectral weight of higher magnetic excitations can be established and quantified. The new generation of high-

intensity neutron sources combined with high-resolution detectors should allow the observation of details of the multimagnon excitation spectrum such as band boundaries, quantitative determination of the dynamical correlation function  $\mathcal{S}(\mathbf{Q}, \omega)$  and discontinuities within a band [8], and weakly bound states just below the band edge. The principle limitation in this approach may be the unavoidable  $\Delta S = 1$  selection rule of magnetic neutron scattering, so that one can only reach spin  $S = 1$  excitations given an  $S = 0$  ground state and an isotropic spin Hamiltonian. Other techniques such as Raman scattering can be used to study certain of these higher excitations, *albeit* with strong constraints on the accessible spin and momentum quantum numbers.

Systems that appear especially interesting for studies of higher magnetic excitations at present are quasi-1D spin chains and spin ladders, since many of these have gaps and hence will have separated bands of higher excitations and perhaps bound states of magnons. The alternating Heisenberg antiferromagnetic chain (AHC) with spin-1/2 is an example of such a system; with any amount of alternation  $0 < \alpha < 1$  (where  $\alpha \equiv J_2/J_1$ ) the AHC has an energy gap in its one-magnon dispersion with a second gap to the multimagnon continuum, and two-magnon bound states with spin-0 and spin-1 are predicted [9]. The AHC is also attractive because of its relative simplicity and because of recent extensive theoretical studies of the low-energy excitations in this model.

In this paper we present results from an inelastic neutron scattering study of higher magnetic excitations in copper nitrate ( $\text{Cu}(\text{NO}_3)_2 \cdot 2.5\text{D}_2\text{O}$ ), which was recently confirmed by neutron scattering [10] to be an accurate realization of a strongly alternating Heisenberg antifer-

romagnetic chain. This material is especially attractive because the alternation parameter  $\alpha \approx 0.27$  is close to the value predicted to maximize the separation of the spin-1 two-magnon bound state from the continuum [11]. In addition it is relatively easy to prepare large single crystals of this material, which compensates for the weak neutron scattering intensity from the higher magnetic excitations.

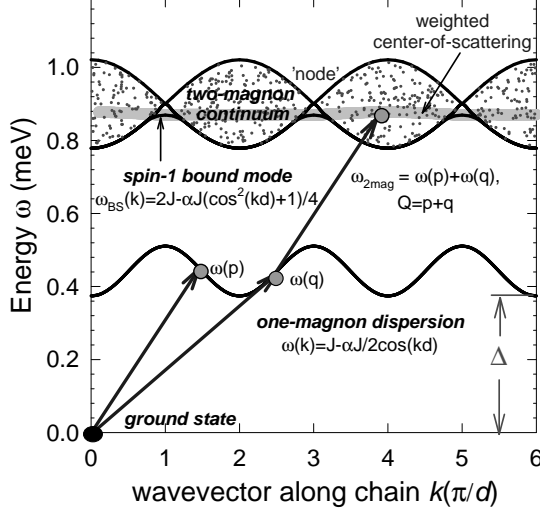


FIG. 1: The  $S = 1$  excitation spectrum of the spin-1/2 alternating Heisenberg chain with moderately strong dimerization. The parameters used are  $J = 0.45$  meV and  $\alpha = 0.27$ , (as fit to copper nitrate neutron scattering data.) There is an energy gap  $\Delta$  from the  $S = 0$  ground state to the  $S = 1$  triplet magnon band. The two-magnon continuum states are also shown; these have energies and wavevectors given by the sum of two independent one-magnon excitations. A  $S = 1$  bound state is predicted to lie just below the two-magnon continuum for small wavevectors near  $k = \pi/d$ , where the continuum has minimum width.

The paper is arranged as follows: Section (2) summarizes important results from the theory of the ground and excited states of the alternating Heisenberg chain. Section (3) reviews the magnetic properties of  $\text{Cu}(\text{NO}_3)_2 \cdot 2.5\text{D}_2\text{O}$ , or CN for short. Section (4) presents the results of our measurements, with the analysis in terms of the model given in section (5). A discussion of the results is given in (6), with conclusions in (7). Additional theoretical results for two-magnon excitations in this model are given in the Appendix.

## THEORY

The spin-1/2 alternating Heisenberg chain has received much attention in the theoretical literature. This simple model plays a central role in the study of the spin-Peierls effect, and is also known to provide an accurate

TABLE I: Eigenstates of dimer  $m$ ,  $H_m = J\mathbf{S}_{m,-} \cdot \mathbf{S}_{m,+}$ .

Label	$\Psi_m$	$E$	$S_m^z$	$S_m$
$G_m$	$\frac{1}{\sqrt{2}} \{  \uparrow\downarrow\rangle -  \downarrow\uparrow\rangle \}$	$-3J/4$	0	0
$1_m$	$ \uparrow\uparrow\rangle$	$J/4$	1	1
$0_m$	$\frac{1}{\sqrt{2}} \{  \uparrow\downarrow\rangle +  \downarrow\uparrow\rangle \}$	$J/4$	0	1
$\bar{1}_m$	$ \downarrow\downarrow\rangle$	$J/4$	-1	1

description of the magnetic properties of many real materials. The model consists of antiferromagnetically coupled Heisenberg spin pairs, “dimers”, which are themselves coupled by weaker antiferromagnetic Heisenberg interactions in an alternating chain, as shown in Fig.2. The Hamiltonian for this model is given by

$$H = \sum_{m=1}^{N/2} J \left\{ \mathbf{S}_{m,-} \cdot \mathbf{S}_{m,+} + \alpha \mathbf{S}_{m,+} \cdot \mathbf{S}_{m+1,-} \right\}, \quad (1)$$

where  $N$  is the number of spins in the chain,  $J > 0$  (also called  $J_1$ ) is the intradimer coupling,  $\alpha J$  (also  $J_2$ ) is the interdimer coupling, and  $\alpha$  is allowed the range  $0 < \alpha < 1$ . The index  $m$  labels the dimers, and  $-$  and  $+$  denote left and right spins. The position of each spin is given by  $\mathbf{r}_{m,\pm} = m\mathbf{d} \pm \boldsymbol{\rho}/2$ , where  $\mathbf{d}$  is the chain repeat vector, and  $\boldsymbol{\rho}$  is the intradimer separation.

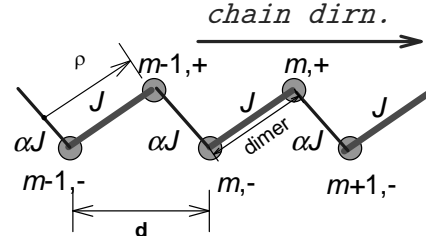


FIG. 2: Alternating chain layout showing dimers coupled together. Each dimer is labeled by an index  $m$ ,  $\boldsymbol{\rho}$  is the separation between dimer spins, and  $\mathbf{d}$  is the chain repeat vector.

This model has a nontrivial spin-0 ground state, and for all  $\alpha$  in the allowed range  $0 < \alpha < 1$  has a gap to the first excitation, which is a band of spin-1 excitations (magnons). In the “strong-coupling limit”  $\alpha \ll 1$  the ground state approaches a system of uncoupled spin-0 dimers, and the one-magnon excitations can be accurately described as a single dimer excited to spin-1 (an “exciton”), delocalized on the chain to give states of definite along-chain wavenumber  $k$ . The energies and some matrix elements of these states have been evaluated as power series in the intradimer coupling  $\alpha$  [11, 12].

To interpret experimental results approximate analytic forms of the wavefunctions and energies are useful and we include calculations of wavefunctions expanded around the single dimer eigenstates in the Appendix. The one-magnon  $S = 1$  triplet has a gap energy  $\Delta = J - \alpha J/2$

and dispersion to  $\mathcal{O}(\alpha)$

$$\omega_{1\text{mag}}(k) = J - \alpha J/2 \cos(kd). \quad (2)$$

This magnon wavefunction can be visualized as a localized wavepacket of magnetic polarization (excitons) along  $x, y$ , or  $z$  carrying total spin-1 travelling through a featureless singlet background with the gap energy coming from the effort expended in breaking a dimer bond.

Approximate wavefunctions for the two-magnon states are given in the Appendix. At large separations the magnons do not overlap and they behave as free particles, however when close they interfere and scatter off each other. In a one dimensional geometry such scattering conserves particle number, energy, and momentum up to a lattice wavevector, and the scattering introduces a momentum dependent phase shift in the scattered wavefunction. The energy of these states (to order  $\mathcal{O}(1/N)$ ) is given by  $\omega_{k_1, k_2}(k) = \omega_{1\text{mag}}(k_1) + \omega_{1\text{mag}}(k_2)$ , where  $k = k_1 + k_2$  is the total wavevector. The resulting continuum using equation (2) is illustrated in Fig. 1 [8].

As well as elastic scattering of magnons, bound states also form. To appreciate their physical origin consider two dimers, both in excited states, coupled by a single interdimer coupling  $\alpha J$ . In the absence of coupling all the double excited states  $S = 0, 1$ , and  $2$  have the same energy  $2J$ . However, the interdimer coupling splits these states. There is an  $S = 2$  quintuplet of energy  $2J + \alpha J/4$  (this energy is higher because the interdimer coupling favours antiferromagnetism whereas the  $S = 2$  states have all spins along the same direction - ferromagnetic). There is also an  $S = 1$  triplet of energy  $2J - \alpha J/4$ , this lowering of energy is purely quantum mechanical and comes from resonance between the two excited dimers. Finally there is an  $S = 0$  singlet of even lower energy,  $2J - \alpha J/2$ , which gains resonance and also antiferromagnetic energy due to the spins in neighboring dimers pointing in opposite directions.

As the  $S = 0$  and  $1$  states with excited dimers neighboring each other have lower energy than two well separated excited dimers (by  $\alpha J/4$  and  $\alpha J/2$  respectively) there is a short range attractive potential. Magnons can be confined within the potential well (bound states) as long as the relative kinetic energy between the magnons is smaller than the interaction energy.

This situation applies to the bound states in the AHC, the  $S = 0$  mode at all wavevectors and the  $S = 1$  mode over limited wavevectors around the node points. These are positions where the kinetic energy is small compared to the binding potential. The  $S = 1$  bound state is visible to neutron scattering and has a dispersion [9][13]

$$\omega_{\text{BS}} = 2J - \frac{\alpha J}{4} (4 \cos^2(kd/2) + 1).$$

The bound state is characterized by a probability amplitude for the separation between the two magnons that

TABLE II: Crystallographic data for  $\text{Cu}(\text{NO}_3)_2 \cdot 2.5\text{H}_2\text{O}$  from reference [15]. The room temperature lattice parameters are  $a = 16.453$ ,  $b = 4.936$ ,  $c = 15.963$  Å and  $\beta = 93.765^\circ$ . The Cu ions are at the 8f positions at (x,y,z) where  $x=0.12613$ ,  $y=0.01352$ ,  $z=0.11376$ . The equivalent positions in the unit cell are:

Atom	$x$ -pos	$y$ -pos	$z$ -pos
1	$x$	$y$	$z$
2	$1 - x$	$1 - y$	$1 - z$
3	$1 - x$	$y$	$\frac{1}{2} - z$
4	$x$	$1 - y$	$\frac{1}{2} + z$
5	$\frac{1}{2} + x$	$\frac{1}{2} - y$	$z$
6	$\frac{1}{2} - x$	$\frac{1}{2} + y$	$1 - z$
7	$\frac{1}{2} - x$	$\frac{1}{2} - y$	$\frac{1}{2} - z$
8	$\frac{1}{2} + x$	$\frac{1}{2} + y$	$\frac{1}{2} + z$

drops exponentially with distance (see appendix for more details). These  $S = 1$  bound states exist only over the range  $|n\pi - kd| \leq \pi/3$ , where  $n$  is an odd integer, see Fig. 1.

## MAGNETIC PROPERTIES OF $\text{Cu}(\text{NO}_3)_2 \cdot 2.5\text{D}_2\text{O}$

The structural and magnetic properties of CN have been thoroughly investigated and shown to be near ideal. The structure of  $\text{Cu}(\text{NO}_3)_2 \cdot 2.5\text{H}_2\text{O}$  was investigated by Garaj [14] and Morosin [15], and was shown to have a monoclinic crystal structure with space group  $I12/c1$  [16] and the lattice parameters and crystallographic copper positions given in Table II. The deuterated form  $\text{Cu}(\text{NO}_3)_2 \cdot 2.5\text{D}_2\text{O}$  we studied has low temperature ( $T = 3$  K) lattice parameters  $a = 16.1$ ,  $b = 4.9$ ,  $c = 15.8$  Å and  $\beta = 92.9^\circ$  [10].

The magnetism of CN arises from the  $\text{Cu}^{2+}$  ions. Crystal electric fields from the oxygen ligands surrounding the  $\text{Cu}^{2+}$  ions quench their orbital moments, leaving a near-isotropic spin-1/2 moment with g-values that show a small easy-axis anisotropy along the crystallographic  $b$ -direction; the values are  $g_{\parallel b} = 2.33$  and  $g_{\perp b} = 2.09$  [17]. Magnetic superexchange in this material is mediated by long double Cu-O-O-Cu exchange paths, which accounts for the rather weak exchange interaction observed in CN.

The exchange couplings of CN were studied by Eckert *et al.* in [18] and are illustrated in Fig. 3. The dominant magnetic exchange integral  $J$  is between pairs of spins (copper positions 7 & 8, and equivalent pairs, *c.f.* Fig. 3) forming dimers with a separation of 5.3 Å. These dimers separated by *crystal vector*  $\mathbf{u} = [u_1, u_2, u_3] \equiv u_1\mathbf{a} + u_2\mathbf{b} + u_3\mathbf{c}$  are coupled together by exchanges  $J'_{\mathbf{u}}$ ; the only exchange paths of appreciable strength are  $J'_{[\frac{1}{2}, \pm\frac{1}{2}, \frac{1}{2}]}$ , connected via bonds between 1 & 7 and equivalent (bond length 6.2 Å). This results in two sets of  $S = 1/2$  alternating Heisenberg chains running in the  $[1, 1, 1]$  and  $[1, \bar{1}, 1]$  directions of the crystal with repetition every

$\mathbf{d} = [1, 1, 1]/2$  and  $\mathbf{d}' = [1, \bar{1}, 1]/2$  respectively (repeat distance  $d = 11.3$  Å); the corresponding intradimer vectors are  $\boldsymbol{\rho} = [0.252, \pm 0.027, 0.228]$  (where the  $x, y, z$  positions from Table II have been used). Inelastic neutron scattering measurements [10] have recently further confirmed the model alternating Heisenberg chain properties of CN and have shown that the dominant collective excitations are indeed the gapped triplet of magnons expected for the AHC.

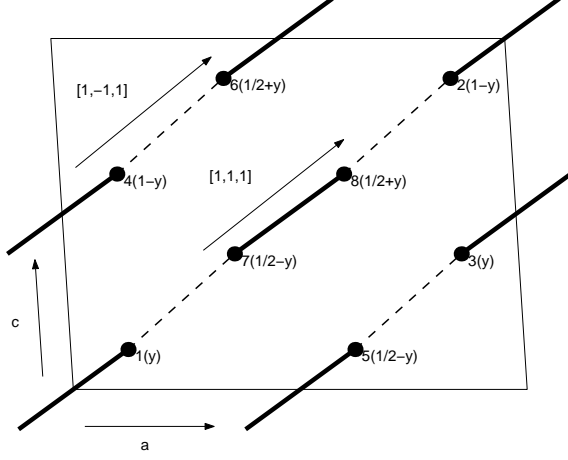


FIG. 3: Positions of copper ions projected onto the  $ac$  plane for  $\text{Cu}(\text{NO}_3)_2 \cdot 2.5\text{D}_2\text{O}$ . The atom positions are those detailed in Table II. Two sets of identical chains run in the  $[1, 1, 1]$  and  $[1, \bar{1}, 1]$  directions respectively.

### Approximate ground state energy

Bulk magnetic measurements give information on the gap, exchange, and ground state energies of the spin chains in copper nitrate. Measurements of the effect of applied magnetic field show that spin flop (SF) ordering is induced in CN above a critical field  $B_{c1} \approx 2.7$  T, with a transition to full alignment at  $B_{c2} \approx 4.3$  T and there are no demagnetization effects in the zero temperature limit [19]. As the orbital moment on the  $\text{Cu}^{2+}$  ions is quenched by the crystal electric field and demagnetization effects are negligible, the field  $B_{c1}$  can be used to directly give the excitation gap energy to the one-magnon states, and Diederix *et al.* report a value of  $\Delta = 0.378 \pm .007$  meV [19].

The gap can be inferred from the transition field because the magnons carry spin quantum numbers  $S^z = 1, 0, -1$  and are split into three dispersive modes shifted by a Zeeman energy with respect to each other. The ground state by virtue of its spin-0 quantum number is unaffected by the field and the transition occurs when the Zeeman energy of the lowest mode closes the gap

and magnons condense into the ground state. The long range order itself is due to weak couplings between the chains.

The high field transition,  $B_{c2}$ , yields further important information. It is where all the low-lying magnons are completely condensed into the ground state and the spins are fully aligned along the field. The fully aligned state is an exact eigenstate, and for an unfrustrated quantum magnet the transition field gives the sum of exchange couplings  $g\mu_B B_{c2} = J + \sum_{\mathbf{u}} J'_{\mathbf{u}} = 0.580 \pm .007$  meV in the system [7]. An estimate of the ground state energy of CN can be made using these numbers.

Using the low temperature isothermal magnetization  $M(B) = g\mu_B \langle S^z \rangle_B$  as a measure of the work required to saturate the spin chains from the zero-field quantum ground state, an energy-per-spin can be inferred. The zero-field ground state energy-per-spin  $e_0$  can be estimated via the formula  $e_0 \approx e_f - g\mu_B S B_{c2} + \int_0^{B_{c2}} M(B) dB$  where the fully-aligned energy-per-spin is  $e_f = S^2/2 \cdot (J + \sum_{\mathbf{u}} J'_{\mathbf{u}}) = g\mu_B B_{c2}/8 = 0.0725 \pm .001$  meV for a  $S = 1/2$  unfrustrated system. Utilizing the 270 mK data of Diederix *et al.* in Fig. 3 of [19] (measured using proton resonance) to determine the integral over magnetization gives an experimental ground state energy-per-spin  $e_0 = -0.174 \pm .004$  meV. This is essentially the  $T = 0$  result, as the gap activation energy corresponds to 4.4 K.

To estimate thermodynamic properties we approximate the sum of the *interdimer* exchanges by the single coupling  $\alpha J = \sum_{\mathbf{u}} J'_{\mathbf{u}}$  of equation (1). Using the  $\mathcal{O}(\alpha^9)$  expansions [11] for  $\Delta(\alpha)$  and  $e_0$  gives  $J = 0.455 \pm .002$  meV and  $\alpha = 0.277 \pm .006$ ; in agreement with the results of [19] and [20],  $J = 0.45$  meV and  $\alpha = 0.27$ . Our calculated values of the thermodynamic parameters  $J + \sum_{\mathbf{u}} J'_{\mathbf{u}} = 0.581$  meV,  $\Delta = 0.379$  meV and  $e_0 = -0.172$  meV agree within error with the experimental values.

## EXPERIMENTAL METHOD

### Neutron scattering

The inelastic neutron-scattering cross-section [21]

$$\frac{d^2\sigma}{d\Omega d\omega} \propto N \sigma_{mag} \sum_{\alpha, \beta} \frac{k_f}{k_i} |F(\mathbf{Q})|^2 (\delta_{\alpha\beta} - Q_\alpha Q_\beta) \mathcal{S}^{\alpha\beta}(\mathbf{Q}, \omega),$$

is proportional to the dynamical response  $\mathcal{S}^{\alpha\beta}(\mathbf{Q}, \omega)$ , where  $\mathbf{Q}$  is the wavevector transfer,  $F(\mathbf{Q})$  is the magnetic form factor,  $N$  is the number of scattering centers, the constant  $\sigma_{mag} = 0.2896$  b,  $k_i$  and  $k_f$  are the momenta of initial and final neutron states respectively,  $g$  is the Landé  $g$ -factor, and  $\alpha = x, y, z$  are Cartesian coordinates. The dynamical response is the space and time

Fourier transform of the spin-spin correlation function

$$S^{\alpha\beta}(\mathbf{Q}, \omega) = \frac{1}{2\pi N} \sum_{i,j} \int \exp(i(\omega t + \mathbf{Q} \cdot (\mathbf{r}_i - \mathbf{r}_j))) \langle S_i^\alpha(0) S_j^\beta(t) \rangle dt,$$

where  $i$  and  $j$  labels sites of the system. For the AHC, equation (1), spin conservation and isotropy in spin space ensure that  $S^{\alpha\beta}(\mathbf{Q}, \omega) = 0$  for  $\alpha \neq \beta$ , and all diagonal spin components are equivalent  $S^{xx}(\mathbf{Q}, \omega) = S^{yy}(\mathbf{Q}, \omega) = S^{zz}(\mathbf{Q}, \omega)$ . At  $T = 0$  this is given by

$$S^{xx}(\mathbf{Q}, \omega) = \frac{1}{2} S^{+-}(\mathbf{Q}, \omega) = \frac{1}{2} \sum_{\lambda} |\langle \Psi_{\lambda}(k) | S_{\mathbf{Q}}^+ | \Psi_G \rangle|^2 \delta(\omega - \omega_{\lambda}),$$

where  $\lambda$  label the eigenstates of  $H$  and

$$S_{\mathbf{Q}}^+ = \frac{1}{\sqrt{2N_d}} \sum_{m=1}^{N_d} \sum_{p=\pm} \exp(i\mathbf{Q} \cdot \mathbf{r}_{m,p}) S_{m,p}^+$$

is the Fourier transformed spin creation operator.

The action of the neutron is to flip a spin and so create a localized spin-1 polarization in the chain, and the strength of scattering to particular states is determined by their overlap with this spin flip state. This means that the multiparticle states will be sampled with particles created close together. This is where interactions of the particle wavefunctions are most important, making neutrons a sensitive technique for looking at overlap effects. An interesting consequence of this is that the short range interactions between particles can have a large influence on measured correlation functions with little effect on the thermodynamics of the spin chain, an effect noted for spinons in uniform chains [22]. Similarly, the thermodynamic influence of bound states at low temperatures vanishes as  $1/N$  yet they have a finite scattering cross section as discussed below.

### Neutron scattering measurements

We made our measurements of the inelastic scattering cross-section of CN using the SPINS cold neutron triple-axis spectrometer at the NIST Center for Neutron Research. The same high quality sample of copper nitrate used by Xu *et al.* [10] was utilized. This 14.1g sample consists of four coaligned single crystals of CN, with deuterium substituting for 92% of hydrogen. The substitution of D for H was made as it reduces significantly the background from incoherent scattering of neutrons but does not change the magnetic properties of the material. The sample was mounted with  $(h, 0, l)$  as the scattering plane in a pumped  $^3\text{He}$  cryostat at a base temperature of 300 mK. This temperature is an order of magnitude smaller than the gap energy ( $\sim 4.4$  K) and the collective

quantum ground state is almost entirely free of thermally produced magnons, with a population of these numbering less than one per two million dimer sites.

The two-magnon scattering is expected to be weak as the neutron matrix element to it is of  $\mathcal{O}(\alpha^2)$  from the ground state so the spectrometer was set up in an open configuration to gain maximum scattered signal, and the only collimator included in the setup was of  $80'$  between monochromator and sample. A vertically focused pyrolytic graphite PG(002) array monochromated the incident neutrons (energy  $E_i$ , wavevector  $\mathbf{k}_i$ ) and a horizontally focused array composed of eleven independently rotatable PG(002) blades was employed to analyze the scattered neutrons ( $E_f$ ,  $\mathbf{k}_f$ ). A cooled Be filter was placed in the incident beam before the sample to remove higher-order contamination from the beam. The actual neutron energy transfer to the sample being  $\hbar\omega = E_i - E_f$  and the wavevector transfer is  $\mathbf{Q} = \mathbf{k}_i - \mathbf{k}_f$ .

Measurements of scattering cross-section were made by fixing the final energy at  $E_f = 2.5$  meV ( $k_f = 1.10 \text{ \AA}^{-1}$ ) and scanning incident energy  $E_i$  at various fixed wavenumber transfers along the chain,  $k = \mathbf{Q} \cdot \hat{\mathbf{d}}$  (i.e. the component of the scattered wavevector along the important chain direction). Although there are actually two types of chain in CN (with repeats  $\mathbf{b} = [1, 1, 1]/2$  and  $\mathbf{b}' = [1, \bar{1}, 1]/2$ ) this is not important in our case - we study the  $(h, 0, l)$  scattering plane where the chains give identical contributions (see Fig. 3).

With an open scattering configuration instrumental resolution is an important consideration. The spectrometer resolution represents the spread in coordinate space  $(\mathbf{Q}, \omega)$  sampled by the instrument at each measured point. The energy resolution of the spectrometer is of Gaussian profile with a full-width-half-maximum (FWHM) at  $E_f = 2.5$  meV and  $\hbar\omega = 0.8$  meV of  $\sim 0.10$  meV. The  $\mathbf{Q}$  resolution is dominated by the wide angular acceptance ( $14^\circ$ ) of the analyzer on the scattered side - it is highly elongated along a direction within the scattering plane that is perpendicular to the scattered wavevector - and approximating the measured angular dependence by a Gaussian profile gives a FWHM of  $\sim 0.2 \text{ \AA}^{-1}$ . This resolution width is very considerable, however by using calculated scan trajectories that maintain the final wavevector  $\mathbf{k}_f$  along the crystallographic  $(1, 0, 1)$  direction, so as to integrate over the nondispersive directions between chains, good wavenumber resolution in  $k$  along the important quantum spin chain directions (estimated at of order  $0.02 \text{ \AA}^{-1}$ ) is maintained.

### RESULTS AND ANALYSIS

Fig. 4 shows some of the results of scans in energy performed on CN: Panel (a) shows a scan at the antiferromagnetic zone-center,  $k = 2\pi/d$ , taken at  $T = 300$  mK. This is the wavenumber along the chain where

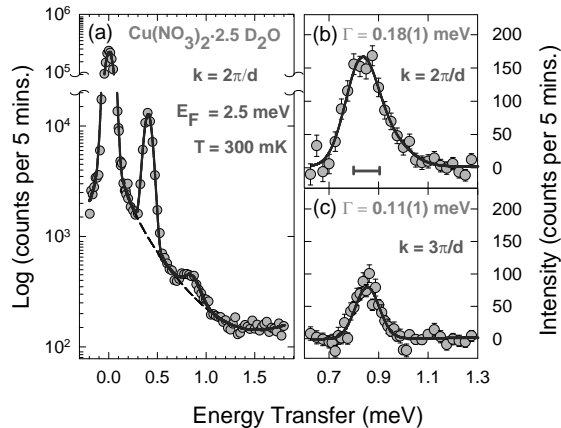


FIG. 4: (a) Low temperature scattering at  $k = 2\pi/d$ . The dashed line is a fitted background and the solid line is a fit to the scattering described in the text. (b) Two magnon scattering with background subtracted off. The solid line is a fit (see text). The solid bar indicates the instrumental resolution. (c) Two-magnon scattering for  $k = 3\pi/d$  with nonmagnetic background subtracted off.

the magnon energy is a minimum, *c.f.* Fig. 1. Strong elastic scattering from incoherent nuclear processes is clearly seen as well as a peak at 0.4 meV as expected for the one magnon mode [10], close to the dimer excitation energy  $J = 0.45$  meV. A second much weaker peak appears at roughly double the dimer energy at about 0.9 meV, which is where two-magnon scattering is expected. On heating up the sample both the 0.4 meV and 0.9 meV peaks disappear identifying these as being magnetic in origin.

Heating up the sample also identifies the non-magnetic background contribution (dashed line in the figure) which consists of the incoherent nuclear peak, modelled by a Gaussian centered at zero-energy, and a broad contribution from thermal diffuse scattering from the analyzer which is well-characterized by a power-times-Lorentzian (broad, quasielastic) component decaying from zero-energy. As the background is large compared to the two magnon signal it was studied in depth at different temperatures and wavevectors.

Panels (b) and (c) of Fig. 4 show this peak with the modelled nonmagnetic background subtracted at  $k = 2\pi/d$  and  $k = 3\pi/d$ , respectively. This feature is considerably weaker than the one-magnon scattering. The FWHM of the peak narrows from 0.18(1) meV at  $2\pi/d$ , panel (b), to 0.11(1) meV at the zone-boundary ( $3\pi/d$ ), panel (c); behavior indeed consistent with two-magnon scattering.

Fig. 1 shows the energy corresponding to a weighted average of scattering as a thick grey line. It is notable that at  $k = 3\pi/d$  to a good approximation the neutrons

couple only to the bound mode, so that nearly all the scattering weight is in it, not the continuum. The calculated neutron scattering intensity from the bound state is  $\sim 2\%$  of the one-magnon intensity which agrees with the data in Fig. 4.

The one- and two-magnon scattering at 300 mK was scanned from  $k = \pi/d$  to  $5\pi/d$  in steps of  $\pi/4d$ . The background subtracted data are plotted in the upper panel of Fig. 5. The lower panel shows the calculated magnetic scattering based on the 1D perturbation theory of the Appendix with the estimated parameters  $J = 0.45$  and  $\alpha = 0.27$ . The calculation includes the correct dimer structure factor effects and uses the true scan trajectories in conjunction with the dimer coordinates given in Table II. Corrections for the  $\text{Cu}^{2+}$  magnetic form factor [23] have also been made. Instrumental line broadening has been included as well by convolving the theoretical calculations with the estimated instrumental resolution and sample mosaic spread. The calculation is directly comparable with the data in the upper panel of Fig. 3, and at a qualitative level there is good agreement with experiment.

Next we consider the measured one- and two-magnon scattering in more detail and relate this to the physical picture presented by perturbation theory. A quantitative comparison between theory and data is shown in Fig. 6. The measured positions of one- and two-magnon peaks are plotted in the left panel. Energies, widths and intensities for each peak were extracted by least-squares fitting of Gaussians. In fact the wavevector and energy resolution was not sufficiently good in this experiment to distinguish details of line shape and the energies, widths and intensities represent the meaningful content of the measured data. We examine the one-magnon scattering first.

#### One-magnon scattering

*Dispersion:* The measured dispersion of the one-magnon states is shown in the left hand panel of Fig. 6. Considerable dispersion of the one-magnon modes around the dimer energy (0.45 meV) is evident as expected. Although the one magnon dispersion has been calculated to high order  $\mathcal{O}(\alpha^5)$  [11] previously, the small value of  $\alpha$  in CN means that the one-magnon dispersion should be well approximated by the  $\mathcal{O}(\alpha)$  result, equation (2). In fact the dispersions in CN measured by Xu *et al.* [10] and Stone *et al.* [24] show that it is well described by

$$\omega(\mathbf{Q}) = J - \frac{1}{2} \sum_{\mathbf{u}} J_{\mathbf{u}} \cos(\mathbf{Q} \cdot \mathbf{u}) \quad (3)$$

with  $J = 0.442(2)$  meV the dimer coupling,  $J_{[111]/2} = 0.106(2)$  meV the along chain coupling, plus additional

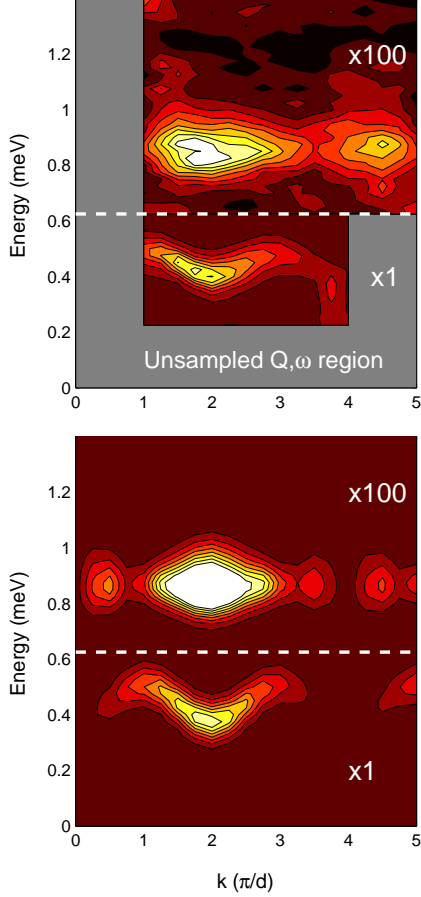


FIG. 5: (Color) Upper panel shows a color filled contour plot of the measured data with nonmagnetic background subtracted. Intensity is on a linear scale indicated by color, going from dark red (minimum) to light yellow (maximum). The two-magnon scattering has been enhanced by a factor of 100 to make it visible on the same scale. Lower panel shows the calculated scattering using perturbation theory with corrections for instrumental resolution, multiple scattering and magnetic form factor.

weak interdimer couplings  $J'_{[1/2,0,0]} = 0.012(2)$  meV and  $J'_{[0,0,1/2]} = 0.018(2)$  meV. The alternation ratio that Xu *et al.* consider  $\alpha = J_{[111]}/J = 0.240(5)$  is smaller than that found from the magnetization data discussed above which is presumably due to the neglect of interchain coupling effects in the analysis of the latter.

The solid line through the one magnon dispersion in Fig. 6 is that calculated using the results of [10] and it gives a reasonable account of the data. The small discrepancies from the peak-centers measured here are attributable due to the effects of the instrumental resolution which averages over a large swathe of the interchain dispersion modulation.

*Intensity:* The lower right-hand panel of Fig. 6 shows the one-magnon intensities extracted from fitting. The neutron scattering matrix element  $S^{+-}(\mathbf{Q}) \equiv$

$|\langle \Psi_{\lambda}(k) | S_{\mathbf{Q}}^{+} | \Psi_G \rangle|^2$  for excitation of the one-magnon states in the AHC to  $\mathcal{O}(\alpha^3)$  is [11]

$$\mathcal{S}_{\text{1mag}}^{+-}(\mathbf{Q}) = (1 - \cos(\mathbf{Q} \cdot \boldsymbol{\rho})) \cdot \left\{ \left( 1 - \frac{5}{16}\alpha^2 - \frac{3}{32}\alpha^3 \right) + \left( \frac{1}{2}\alpha - \frac{1}{8}\alpha^2 - \frac{5}{192}\alpha^3 \right) \cos(kd) + \left( \frac{3}{16}\alpha^2 + \frac{7}{48}\alpha^3 \right) \cos(2kd) + \frac{5}{64}\alpha^3 \cos(3kd) \right\}. \quad (4)$$

The leading order scattering process is from the bare dimer component of the ground state, and the  $\alpha/2 \cdot \cos(kd)$  component in the one magnon structure factor arises from an  $\mathcal{O}(\alpha)$  two-dimer excitation in the ground state. The dynamical structure factor then reflects both the composition of the ground and excited states leading to a complex wavevector dependence.

An interesting aspect of the one-magnon intensity  $\mathcal{S}_{\text{1mag}}^{+-}(\mathbf{Q})$  noted in [11] is that the spin structure factor comes in only as a  $(1 - \cos(\mathbf{Q} \cdot \boldsymbol{\rho}))$  modulation. So where  $\mathbf{Q} \cdot \boldsymbol{\rho} = 2\pi n$  ( $n$  integer) the magnetic intensity should be zero. Although this situation occurs for the measurements at the wavenumber  $k = 3.9\pi/d$ , the scattering does not go to zero because of residual intensity from secondary elastic scattering from incoherent processes. Such residual scattering was also observed in CN by Xu *et al.* [10]. The solid line in the figure then is the scattering intensity predicted using equation (4) with  $J = 0.45$  meV and  $\alpha = 0.27$  including secondary scattering, as well as instrumental resolution and magnetic form factor. It is seen to account very well for the observed scattering intensity. We now consider the two-magnon scattering.

#### Two-magnon scattering

Integrated peak intensities, widths and positions extracted using the fitting method described above for the two-magnon scattering are also plotted in Fig. 6. The peak positions are plotted in the left panel of Fig. 6 (filled circles). They are nearly dispersionless at an energy of  $\sim 0.86$  meV. The peak widths are plotted in the top right-hand panel. These are largest around  $k = 2\pi/d$  and  $4\pi/d$  where the continuum is expected to be widest, and are near resolution limited around  $\pi/d$ ,  $3\pi/d$ , and  $5\pi/d$ . Also shown is the integrated peak intensity  $\int d\omega I(\omega)$ , where  $I(\omega)$  is the intensity, which peaks around  $k = 2\pi/d$ .

*Intensity:* The integrated peak intensity of the measured two magnon scattering includes a sum over the two-particle continuum and  $S = 1$  bound mode. Taking account of the density of momentum states with energy transfer, the scattering intensities for the continuum (eqn. (17)) and bound (eqn. (18)) states as described in the Appendix were computed. As interchain effects are effectively integrated over in the two-magnon scattering, and this results in line broadening rather than shifts in energy; we thus have implicitly included interchain coupling effects in our definition of  $\alpha = 0.27$  for (1).

The energy integrated two-magnon intensity,  $\int d\omega I(\omega)$ , (right middle panel) shows a more complicated  $k$  dependence than the one magnon scattering. The comparison with the  $\mathcal{O}(\alpha^2)$  calculation looks qualitatively similar to the data, however it underestimates the scattering at  $k \approx 9\pi/2d$  and overestimates it at  $2\pi/d$ , which may indicate that higher order terms in the scattering amplitude are important. It is notable that the two-magnon intensity is very strongly dependent on the spatial arrangement of magnetic ions.

*Center:* the fitted peak centers are compared with the computed weighted center  $\langle\omega\rangle = \int d\omega I(\omega) \times \omega$  (gray band) for the  $\mathcal{O}(\alpha^2)$  perturbation theory in the left panel of Fig. 6. The nearly dispersionless extracted positions (grey filled circles) are located at the calculated weighted-average energies (grey band) replotted from Fig. 1. The fact that the weighted center lies below the center of the continuum is a direct result of the movement of scattering weight towards the lower boundary due to the magnon-magnon interaction.

*Width:* the peak widths obtained from the fits are shown in the top right-hand panel. The solid line represents that calculated using the perturbation theory. It is the sum-in-quadrature of the instrumental resolution width in energy and the variance  $\sigma$  of the theoretical intensity where  $\sigma^2 = \int d\omega I(\omega) \times (\omega - \langle\omega\rangle)^2$ . The calculation is seen to provide a good account of the data.

*Bound mode:* One of the most interesting aspects of the multiparticle states in the AHC is the existence of the bound mode below the two-magnon continuum. The predicted wavevector dependence of the intensity (see Appendix) is

$$\mathcal{S}_{\text{BS}}^{+-}(\mathbf{Q}) = \left(\frac{\alpha}{4}\right)^2 [1 - 4 \cos^2(kd/2)] \times [\sin(\mathbf{Q} \cdot (\boldsymbol{\rho} + \mathbf{d})/2) + 3 \sin(\mathbf{Q} \cdot (\boldsymbol{\rho} - \mathbf{d})/2)]^2.$$

and should be visible around  $k = 3\pi/d$ . The binding energy of the  $S = 1$  state, neglecting interchain coupling, is predicted to be [11]  $E_B = J(\frac{1}{4}\alpha - \frac{13}{32}\alpha^2) = 0.017$  meV for CN. The scattering in CN around  $k = 3\pi/d$  is centered at  $0.852 \pm .007$  meV, which gives a binding energy of  $E_B = 0.03 \pm .02$  meV. In addition the scattering is near resolution limited, as expected for a well-defined mode. However, although the energy and intensity around  $k = 3\pi/d$  lend support to binding around this bandwidth minimum, the experimental error means this does not constitute definitive proof of the effect in CN.

## DISCUSSION

Our measurements establish the feasibility of studying weak multi-magnon states using neutron scattering and raise a number of important issues. Firstly the introduction of experimental data highlights the need for

practical techniques for calculating the multiparticle excitation spectra and cross sections for realistic spin models. Our perturbation theory, although useful for interpreting results, is of too low order to quantitatively account for our measurements and in addition does not include interchain coupling. Very powerful linked-cluster-expansion techniques have recently been introduced that allow multiparticle spectra to be calculated to high order[25, 26] for the AHC and the extension of these to calculations of the neutron scattering cross-section would be a significant development. Analytical approaches based on Green function techniques may also prove fruitful. Secondly, measurement of weak multiparticle signals precludes the access of neutron scattering to measuring bound two-magnon states. Interactions such as next nearest neighbor coupling should further stabilize bound modes and make measurement of these easier. A question which requires further investigation is the stability of such bound modes to thermal fluctuations and also interchain coupling. An alternative route for investigating the phenomenology of particle binding is through solitonic systems such as the 1D Ising chain with small XY-like terms [27]. In this case the coupling of neutrons to pairs of  $S = 1/2$  solitons (also called spinons) is at zeroth order and therefore strong. Binding of solitons only occurs when extra terms are included in the Hamiltonian, such as exchange mixing [28], next-nearest neighbor coupling [29], or transverse field [30]. Evidence for this binding phenomenon in and Ising-like chain has been observed recently in neutron scattering experiments [28].

Time-of-flight (TOF) neutron spectrometers give potentially much better energy resolution than conventional triple-axis instrumentation and could provide definitive proof of the bound state in the alternating chain by resolving the bound mode from the continuum. Previously, TOF techniques have proven successful in the study of similar binding effects at the bandwidth minimum of the two-soliton continuum scattering of the  $S = 1/2$  XXZ Ising chain material CsCoCl<sub>3</sub> [28]. Although limited neutron fluxes may make such measurements difficult for CN [10] these should be feasible and we plan to make such measurements in the near future.

## SUMMARY

In summary, we have used inelastic neutron scattering to investigate the ground and excited states of the near-ideal alternating Heisenberg chain material Cu(NO<sub>3</sub>)<sub>2</sub> · 2.5D<sub>2</sub>O, and also derived the scattering analytically to lowest order in perturbation theory. Our measurements are consistent with the predictions of this model for several magnetic properties of this system, including the ground state energy, one- and two-magnon excitation spectra and intensities, and possibly the existence of a



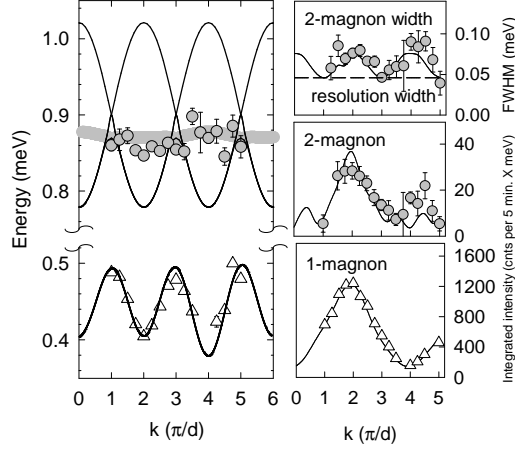


FIG. 6: Comparison of theory and data. Left panel shows fitted positions of observed scattering using perturbations theory (see text). Right lower panel shows fitted one magnon intensity compared with perturbation theory (see text). Right upper panel shows a comparison of the two-magnon intensity with perturbation theory (see text).

two-magnon bound state. Much experimental work remains to be done to establish the phenomenology of binding in isotropic 1D systems.

We wish to thank Drs B. Lebeck, R. Hazell, B. Lake, P-A Lindgård, and D. McMorro for their help and advice and also Risø National Laboratory for generous support. This work was partly supported by Oak Ridge National Laboratory, managed by UT-Battelle, LLC, for the US Dept. of Energy under contract DE-AC05-00OR22725. The NSF supported work at SPINS through DMR-9423101 and work at JHU through DMR-9453362 and DMR-9801742. DHR acknowledges the generous support of the David and Lucile Packard Foundation. Work at Harvard (KD) was supported by NSF-DMR grants 9981283, 9714725, and 9976621

## APPENDIX

### Ground state

Here we apply the perturbation theory of [11] to two-magnon scattering. The single dimer eigenstates (labelled  $G, 1, 0, \bar{1}$ ) are listed in Table I and the ground state of the uncoupled dimers ( $\alpha = 0$ ) is a direct product of dimer ground states

$$\Psi_0 = \prod_{m=1}^{N_d} |G_m\rangle, \quad E_0 = -\frac{3JN_d}{4}. \quad (5)$$

As total spin  $S_T = \sum_{m=1}^{N_d} S_m$ , and  $S_T^z = \sum_{m=1}^{N_d} S_m^z$  are constants-of-the-motion for the Hamiltonian  $H$  they organize the Hilbert space. For notation we introduce dimer creation operators  $a_m^+ |G_m\rangle = |a_m\rangle$  where  $a = 1, 0, \bar{1}$  label excited dimer states. In real space we denote the singly excited states with quantum numbers  $(S_T, S_T^z) = (1, a)$  as  $|a\rangle_m = a_m^+ \Psi_0$  and the doubly excited with  $|(S_T, S_T^z)\rangle_{m,\nu}$  as the Clebsh-Gordan combinations of excitations at dimer sites  $m$  and  $m + \nu$  i.e.  $|(0, 0)\rangle_{m,\nu} = 1/\sqrt{3}\{1_m^+ \bar{1}_{m+\nu}^+ - 0_m^+ 0_{m+\nu}^+ + \bar{1}_m^+ 1_{m+\nu}^+\} \Psi_0$ ,  $|(1, 1)\rangle_{m,\nu} = 1/\sqrt{2}\{0_m^+ 1_{m+\nu}^+ - 1_m^+ 0_{m+\nu}^+\} \Psi_0$ , etc.

As the alternating chain has translational symmetry plane-wave states prove convenient

$$|a\rangle_k \equiv \frac{1}{\sqrt{N_d}} \sum_{m=1}^{N_d} e^{imkd} |a\rangle_m, \quad (6)$$

and

$$|(S, S^z)\rangle_{k,\nu} \equiv \frac{1}{\sqrt{N_d}} \sum_{m=1}^{N_d} e^{imkd} |(S, S^z)\rangle_{m,\nu}. \quad (7)$$

where the allowed momenta are  $k_n = 2n\pi/N_d d$ , where  $n$  are integers from  $-N_d/2$  to  $N_d/2$ . The action of the Hamiltonian on the basis states has been considered in [11] and the ground state to  $\mathcal{O}(\alpha)$  is

$$\Psi_G = \eta_0 [\Psi_0 - \alpha \frac{\sqrt{3}}{8} \sum_{m=1}^{N_d} |(0, 0)\rangle_{m,1}] \quad (8)$$

where  $\eta_0 = 1 - (3/128)\alpha^2 N_d$ .

Neutron scattering measures the square of the expectation value of the spin operator  $S^+(\mathbf{Q}) = (2N_d)^{-1/2} \sum_{m=1}^{N_d} \sum_{p=\pm} \exp(i\mathbf{Q} \cdot \mathbf{r}_{m,p}) S_{m,p}^+$  between eigenstates, where  $\mathbf{Q}$  is the wavevector transfer of the neutron. The action of this spin operator applied to the ground state is

$$\begin{aligned} S^+(\mathbf{Q}) |\Psi_G\rangle &= A_{\mathbf{Q}} |1\rangle_k + B_{\mathbf{Q}} |(1, 1)\rangle_{k,1}, \\ A_{\mathbf{Q}} &= \frac{1}{\sqrt{2}} (e^{i\mathbf{Q} \cdot \boldsymbol{\rho}/2} - e^{-i\mathbf{Q} \cdot \boldsymbol{\rho}/2}) (1 + \frac{\alpha}{4} \cos(kd)), \\ B_{\mathbf{Q}} &= \frac{\alpha}{8} (e^{i\mathbf{Q} \cdot \boldsymbol{\rho}/2} + e^{-i\mathbf{Q} \cdot \boldsymbol{\rho}/2}) (e^{ikd} - 1). \end{aligned} \quad (9)$$

where  $k = \mathbf{Q} \cdot \hat{\mathbf{d}}$  is the wavenumber of the states excited by this operator. The neutron scattering matrix element at  $T = 0$  to state  $\lambda$ , is given by  $S_{\lambda}^{+-}(\mathbf{Q}) = \left| \langle \Psi_{\lambda} | S_{\mathbf{Q}}^+ | \Psi_G \rangle \right|^2$ .

### One-magnon states

The one-magnon wavefunctions to order  $\mathcal{O}(\alpha)$  are [11]

$$\begin{aligned} \Psi_{1\text{mag}} &= |a\rangle_k + \frac{\alpha}{2\sqrt{2}} (e^{ikd} + 1) |(1, a)\rangle_{k,1} - \\ &\quad \frac{\alpha\sqrt{3}}{8\sqrt{N_d}} \sum_{m,m'=1}^{N_d} \delta_{m \neq m'} e^{imkd} a_m^+ |(0, 0)\rangle_{m',1} \end{aligned} \quad (10)$$

and form an  $S = 1$  triplet with an energy gap  $\Delta = J - \alpha J/2$  above the ground state and dispersion

$$\omega_{1\text{mag}}(k) = J - \alpha J/2 \cos(kd). \quad (11)$$

Application of the  $S^+(\mathbf{Q})$  operator gives the intensity to  $\mathcal{O}(\alpha)$

$$\mathcal{S}_{1\text{mag}}^{+-}(\mathbf{Q}) = (1 - \cos(\mathbf{Q} \cdot \boldsymbol{\rho})) \cdot \left\{ 1 + \frac{1}{2} \alpha \cos(kd) \right\}.$$

### Two-magnon states

Ignoring states higher than two-excited-dimer (as they do not contribute to the neutron-scattering matrix element to lowest order in  $\alpha$ ), the action of the Hamiltonian is [11]

$$H|a\rangle_k = \alpha_k |a\rangle_k + \sqrt{2} \gamma_k^\dagger |(1, a)\rangle_{k,1}$$

and

$$H|(1, a)\rangle_{k,\nu} = \begin{cases} \sqrt{2} \gamma_k |a\rangle_k + (\beta - \epsilon) |(1, a)\rangle_{k,1} + \gamma_k |(1, a)\rangle_{k,2}, & \nu = 1 \\ \beta |(1, a)\rangle_{k,\nu} + \gamma_k |(1, a)\rangle_{k,\nu+1} + \gamma_k^\dagger |(1, a)\rangle_{k,\nu-1}, & \nu > 1 \end{cases} \quad (12)$$

where  $\alpha_k = J - (\alpha J/2) \cdot \cos(kd)$ ,  $\beta = 2J$ ,  $\epsilon = \alpha J/4$ ,  $\gamma_k = -\frac{\alpha J}{4} (1 + e^{-ikd})$ , and  $\dagger$  denotes complex conjugation. The excitation spectrum can be calculated by direct diagonalization of a large number of dimers and application of the matrix element above or by analytical solution.

Approximate analytical wavefunctions for the  $S = 1$  states can be calculated using elementary scattering theory, see [29]. Ignoring the coupling to the one-excited-dimer states for the time being, the two-magnon wavefunctions are

$$\Psi_{2\text{mag}}(k) = \sum_{\nu=1}^{N_d-1} b_\nu \exp(i\theta\nu) |(1, 1)\rangle_{k,\nu}. \quad (13)$$

where for  $\theta = -i \log(\sqrt{\gamma_k^\dagger / \gamma_k}) = kd/2$  the time-independent Schrödinger equation reduces to solving the real and symmetric system of equations

$$\begin{aligned} \lambda b_1 &= (\beta - \epsilon) b_1 + \tilde{\gamma}_k b_2 \\ &\vdots \\ \lambda b_\nu &= \beta b_\nu + \tilde{\gamma}_k (b_{\nu+1} + b_{\nu-1}) \\ &\vdots \\ \lambda b_{N_d-1} &= (\beta - \epsilon) b_{N_d-1} + \tilde{\gamma}_k b_{N_d-2} \end{aligned} \quad (14)$$

where  $\tilde{\gamma}_k = \sqrt{\gamma_k^\dagger \gamma_k} = \alpha J/2 \cdot |\cos(kd/2)|$  and the term  $\exp(i\theta\nu)$  serves to transform to the center-of-momentum (center  $R$ ) frame where magnons are at  $r_i = R - \nu/2$  and  $r_j = R + \nu/2$  with total momentum  $K = k_1 + k_2 = kd$ .

### Magnon-pair-state solutions

Magnon-pair-states comprise particles that are free at large distances and for particle conservation in one-dimension the interactions introduce a phase factor  $\phi$  on scattering. This state corresponds to

$$b_\nu^\mu = X_0 (\exp(ip_\mu \nu) - \exp(-i(p_\mu \nu - \phi_\mu))) \quad (15)$$

where the normalization constant  $X_0 \simeq 1/\sqrt{N_d}$ ,  $p_\mu$  is the relative momentum, and  $\mu = 1, 2, \dots, N_d - 1$  index the eigenstates. The phases and momenta are determined by the boundary conditions of the particles and their interaction energy. The standard method of solving for these boundary conditions [29, 31] is to introduce the single site coefficients  $b_0$  and  $b_{N_d}$  and set  $\epsilon b_1 = \tilde{\gamma}_k b_0$  and  $\epsilon b_{N_d-1} = \tilde{\gamma}_k b_{N_d}$  and substitute into equation (14). The momentum  $p_\mu$  and phase  $\phi_\mu$  solve for the constraints on  $b_0$  and  $b_{N_d}$  when

$$e^{i\phi_\mu} = \frac{\tilde{\gamma}_k + \epsilon \exp\left(-i \frac{\pi\mu + \phi_\mu}{N_d}\right)}{\tilde{\gamma}_k + \epsilon \exp\left(i \frac{\pi\mu + \phi_\mu}{N_d}\right)}, p_\mu = \frac{\pi\mu + \phi_\mu}{N_d} \quad (16)$$

and the eigenvalues are  $\lambda_\mu = 2J - \alpha J \cos(kd) \cos(p_\mu) + \mathcal{O}(1/N_d)$ . In the time-dependent Schrödinger picture this state corresponds to two particles with wavepackets at positions  $r_i = R + \nu/2$  and  $r_j = R - \nu/2$  and with momenta  $k_1 = (K + p)/2$  and  $k_2 = (K - p)/2$  that scatter via the  $\mathbf{S}$ -matrix  $\mathbf{S}_{k_1, k_2} = -\exp(i\phi_{k_1 - k_2})$ , and the eigen-spectrum is

$$\omega_{k_1, k_2} = \omega_{1\text{mag}}(k_1) + \omega_{1\text{mag}}(k_2) \quad (17)$$

with  $\omega_{1\text{mag}}(k) = J - \alpha J/2 \cdot \cos(kd)$  as above.

Including the coupling to the  $|1\rangle_k$  states as a perturbation gives the approximate wavefunction

$$\Psi_{2\text{mag}}(k, \mu) = -\frac{\alpha c_1^\mu}{2\sqrt{2}} (1 + e^{-ikd}) |1\rangle_k + \sum_{\nu=1}^{N_d-1} c_\nu^\mu |(1, 1)\rangle_{k,\nu} \quad (18)$$

where  $c_\nu^\mu = b_\nu^\mu \exp(ikd\nu/2)$ . The neutron scattering matrix element can then be computed straightforwardly for a large  $N_d$  system by evaluating the closure with equation (8).

### Bound state solutions

When  $\tilde{\gamma}_k < \epsilon$ ,  $\phi_\mu$  cannot be solved with  $\mu = 1$  and  $N_d - 1$ , and the  $c_\nu^1$  and  $c_\nu^{N_d-1}$  solutions comprise exponentially decaying bound states solutions below the two magnon continuum. The  $S = 1$  bound state wavefunctions and energy have previously been given by Ührig and Schulz

[9], and Damle and Nagler [13]. It is specified by equation (18) with

$$b_\nu^1 = \sqrt{\frac{\epsilon^2 - \tilde{\gamma}_k^2}{\tilde{\gamma}_k^2}} \exp(-\kappa\nu), \quad (19)$$

where  $\exp(-\kappa) = -\tilde{\gamma}_k/\epsilon$  which has dispersion energy

$$\omega_{\text{BS}} = 2J - \frac{\alpha J}{4} (4 \cos^2(kd/2) + 1).$$

An interesting feature of the bound state solution is that it only exists over the range  $|n\pi - kd| \leq \pi/3$ , where  $n$  is an odd integer, and so there is an  $S = 1$  bound mode only for small wavevectors around the narrowest part of the continuum. Using our wavefunction we calculate the neutron scattering strength from the bound state to be

$$\mathcal{S}_{\text{BS}}^{+-}(\mathbf{Q}) = \left(\frac{\alpha}{4}\right)^2 [1 - 4 \cos^2(kd/2)] \times [\sin(\mathbf{Q} \cdot (\boldsymbol{\rho} + \mathbf{d})/2) + 3 \sin(\mathbf{Q} \cdot (\boldsymbol{\rho} - \mathbf{d})/2)]^2.$$

- 
- [1] A. Oosawa *et al.*, Physica B **294-295**, 34 (2001).
  - [2] T. Nikuni *et al.*, Phys. Rev. Lett. **84**, 5868 (2000).
  - [3] B. C. Watson *et al.*, Phys. Rev. Lett. **86**, 5168 (2001).
  - [4] W. Yu and S. Haas, Phys. Rev. B **62**, 344 (2000).
  - [5] T. Giamarchi and A. M. Tsvelik, Phys. Rev. B **59**, 11398 (1999).
  - [6] I. Affleck, Phys. Rev. B **43**, 3215 (1991); E. Sorensen and I. Affleck, Phys. Rev. Lett. **71**, 1633 (1993).
  - [7] R. Coldea, D.A. Tennant, K. Habicht, P. Smeibidl, C. Wolters and Z. Tylczynski, Phys. Rev. Lett. **88**, 7203 (2002).
  - [8] T. Barnes, cond-mat/0204115 (unpublished).
  - [9] G.S. Uhrig and H.J. Schulz, Phys. Rev. B **54**, R9624 (1996).

- [10] G. Xu, C. Broholm, D.H. Reich, and M.A. Adams, Phys. Rev. Lett. **84**, 4465 (2000).
- [11] T. Barnes, J. Riera, and D.A. Tennant, Phys. Rev. B **59**, 11384 (1999).
- [12] R.R.P. Singh and Z. Weihong, Phys. Rev. B **59**, 9911 (1999).
- [13] K. Damle and S. Sachdev, Phys. Rev. B **57**, 8307 (1998); K. Damle and S.E. Nagler, cond-mat/9904438 (unpublished).
- [14] J. Garaj, Acta Chem. Scand. **22**, 1710 (1968).
- [15] B. Morosin, Acta Crystallogr. Sect. B **26**, 1203 (1970).
- [16] Note that the space group for  $\text{Cu}(\text{NO}_3)_2 \cdot 2.5\text{H}_2\text{O}$  has been incorrectly given in previous work as  $I 1 2/a 1$ .
- [17] K.M. Diederix, J.P. Groen, J.S.J.M. Hekens, T.O. Klaassen, and N.J. Poulsen, Physics B **93**, 99 (1978).
- [18] J. Eckert *et al.* Phys. Rev. B **20**, 4596 (1979).
- [19] K.M. Diederix *et al.* Phys. Rev. B **19**, 420 (1979).
- [20] J.C. Bonner *et al.* Phys. Rev. B **27**, 248 (1983).
- [21] W. Marshall and S.W. Lovesey, *Thermal Neutron Scattering* (Clarendon, Oxford, 1971).
- [22] B.A. Bernevig, D. Giuliano, and R.B. Laughlin, Phys. Rev. Lett. **86**, 3392 (2002).
- [23] P.J. Brown, in *International Tables for Crystallography*, edited by A.J.C. Wilson and E. Prince (Kluwer Academic Publishers, Boston, 1999), Vol. C.
- [24] M. Stone *et al.* unpublished.
- [25] S. Trebst, H. Monien, C.J. Hamer, W.H. Zheng, R.R.P. Singh, Phys. Rev. Lett. **85**, 4373 (2000).
- [26] W.H. Zheng, C.J. Hamer, R.R.P. Singh, S. Trebst, H. Monien, Phys. Rev. B **63**, 144410 (2001).
- [27] N. Ishimura and H. Shiba, Prog. Theor. Phys. **63**, 743 (1980).
- [28] J.P. Goff, D.A. Tennant, and S.E. Nagler, Phys. Rev. B **52**, 15992 (1995).
- [29] F. Matsubara, and S. Inawashiro, Phys. Rev. B **43**, 796 (1991).
- [30] A. Ghosh, J. Phys. Condens. Matter **13**, 5205 (2001).
- [31] D.C. Mattis, "The Theory of Magnetism I", Chapter 5, Springer-Verlag (Berlin) 1988.